ACS APPLIED MATERIALS & INTERFACES

RESEARCH ARTICLE

www.acsami.org

Understanding the Improved Stability of Hybrid Polymer Solar Cells Fabricated with Copper Electrodes

B. Reeja-Jayan and Arumugam Manthiram*

Materials Science and Engineering Program, The University of Texas at Austin, Austin, Texas 78712, United States

Supporting Information

ABSTRACT: It is known that atmospheric oxygen is essential for realizing the photovoltaic properties of P3HT−TiO_2-based hybrid polymer solar cells because oxygen vacancies created in TiO_2 can become recombination sites for charge carriers, causing photovoltaic properties like open-circuit voltage (V_{oc}) to decline quickly in an inert atmosphere. We demonstrate here that using an annealed Cu layer as hole collecting electrode results in a remarkably stable hybrid solar cell that maintains its photovoltaic parameters during 1 h of continuous testing in an inert atmosphere. An analysis of the data from photovoltaic device performance tests and X-ray photoelectron spectroscopy (XPS) attributes this improvement to the tendency of Cu to form sulfide-like complexes with the S atoms on P3HT, thereby inducing a chemically driven vertical segregation of P3HT toward the hole-collecting metal electrode. Additionally, XPS depth profiling analysis shows that Cu atoms can diffuse up to the TiO_2 layer and assist in filling up oxygen vacancies on the TiO_2 surface, thus eliminating defects that can act as donors of free electrons and degrade photovoltaic performance in an inert atmosphere. We analyze these improvements by examining in situ the effect of Cu on the P3HT and TiO_2 layers and on the organic−inorganic interface formed between them inside a hybrid solar cell.

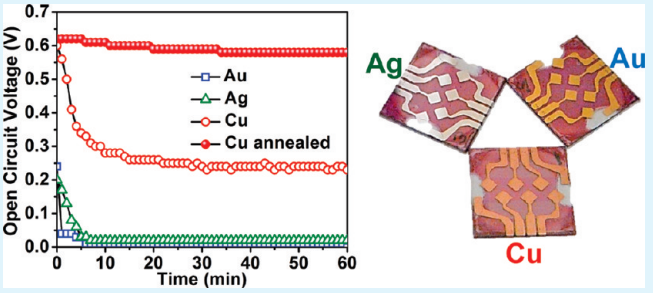

KEYWORDS: hybrid solar cells, P3HT−TiO_2 cells, interface, metal electrode, stability, oxygen vacancies

1. INTRODUCTION

The major advantage of organic photovoltaics is their compatibility with conventional printing and coating techniques, making them cost-effective and suitable for large scale deployment.[1−6] Organic or polymer solar cells can become commercially viable only if both solar energy conversion efficiency and operational stability can be improved while keeping fabrication costs low. Of the various types of organic solar cells, hybrid polymer solar cells comprising organic−inorganic nanocomposite heterojunctions are perhaps the least understood.[7−13] This is mainly because of the complex and, in some cases, peculiar properties of the interface between the organic and inorganic components in such solar cells. This work investigates the hybrid solar cell systems comprising poly(3-hexylthiophene) (P3HT) as the electron-donating, light-absorbing polymer (organic) and nanocrystalline titanium dioxide (TiO_2) as the electron acceptor (inorganic).[1,14−18]

Sunlight is harvested by P3HT to form Coulombically bound frenkel excitons, which then dissociate because of the difference in energy between the polymer and the inorganic nanocrystals. As depicted in Figure 1, the electron hops into and moves through the nanocrystalline TiO_2 network, while the hole is transported by P3HT. Although this mechanism may seem deceptively simple, the interface between P3HT and TiO_2 is far from ideal and the exact nature of these charge separation and transfer processes at this organic−inorganic junction is an ongoing area of research.[1,3,7−18] It has been reported that atmospheric oxygen is essential for establishing the photovoltaic properties of the polymer−TiO_2-based p−n junction, as properties like open-circuit voltage (V_{oc}) decline quickly in an inert atmosphere.[7,9−12]

The organic−inorganic interface in hybrid solar cells is characterized by a depletion region, which has been reported to be the origin of the open-circuit voltage (V_{oc}) of these solar cells.[9] In fact, V_{oc} can be approximated by the energy difference between the highest occupied molecular orbital (HOMO) of P3HT and the conduction band edge (E_c) of TiO_2.[16] One of the interesting aspects of transition metal oxides like TiO_2 is that the surface of these oxides tends to quickly lose oxygen and form $TiO_{2-\delta}$ with a reduction of Ti^{4+} to Ti^{3+}.[9−11] This process is particularly accelerated in vacuum or inert atmosphere, resulting in the generation of a large number of oxygen vacancies and Ti^{3+} on the surface of TiO_2. This results in the formation of defect states that pushes the Fermi level of the oxide surface downward into the electronic band gap.[9,10,19] Removing oxygen also shifts the Fermi level of P3HT upward into the band gap away from the HOMO level.[20] As seen in Figure 2, coupling these two changes will result in a reduction of the contact potential at the P3HT−TiO_2 interface, thereby lowering the V_{oc} and degrading

Received: January 19, 2011
Accepted: March 30, 2011
Published: March 30, 2011

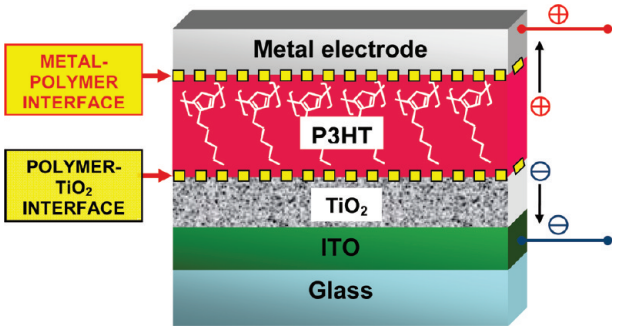

Figure 1. Schematic of an interfacial prototype of P3HT−TiO_2 hybrid solar cell.

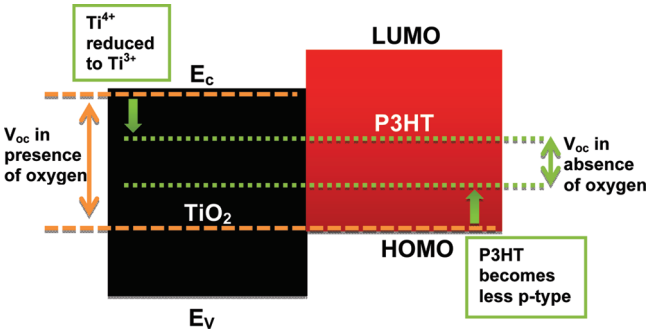

Figure 2. Energy band diagram of P3HT−TiO_2 (organic−inorganic) hybrid interface.

the photovoltaic effect in the absence of oxygen. On exposing the cell to air, the oxygen vacancies in TiO_2 are filled up and the entire process is reversed.[9−13] This might seem to suggest that it is advisible to operate these cells under ambient conditions. However, while oxygen is needed to maintain the balance of oxide ions in TiO_2, oxygen can damage polymers like P3HT by photobleaching in the long run.[21] Furthermore, commercial solar cells are always encapsulated in order to protect them from weather, moisture, and dust, thereby making it imperative that the polymer−TiO_2 interface operates efficiently in an environment devoid of oxygen. Hybrid polymer solar cells can become a commercial reality only if this degradation of photovolatic properties triggered by the dynamic changes taking place inside such devices in the absence of oxygen can be overcome.

We reported recently that the use of Cu as the top hole collecting electrode improves the stability of P3HT−TiO_2-based hybrid solar cells in the absence of oxygen.[22] We demonstrate here that annealing the Cu electrode results in a remarkably stable hybrid solar cell that maintains its photovoltaic parameters during 1 h of continuous testing in an inert atmosphere. This improvement can be attributed to strong interfacial chemical bonding between Cu and S atoms of P3HT to form copper−sulfur complexes or copper sulfide like species as indicated by photoelectron spectroscopic (XPS) data. Such a chemically driven vertical segregation of P3HT toward the hole-collecting Cu electrode selectively directs holes toward the Cu electrode, thereby reducing recombinations. In this work, we use XPS depth profiling analysis to show that in addition to bonding with P3HT, these Cu atoms can diffuse up to the TiO_2 layer and fill up oxygen vacancies on the TiO_2 surface, thereby eliminating defects that can act as donors of free electrons and degrade photovoltaic performance in an inert atmosphere.

We combine data from photovoltaic device performance tests with XPS depth profiling to shed light on the delicate equilibrium that exists between atmospheric oxygen and the oxide ions within the TiO_2 lattice. The combination of depth profiling and excellent depth resolution makes XPS a powerful tool to examine in situ the nature of the P3HT and TiO_2 layers separately and to investigate the interfaces between them (Figure 1).

2. EXPERIMENTAL SECTION

2.1. Materials. Tetrabutyl titanate (TBT) [$Ti(OC_4H_9)_4$] and 2,4-pentanedione were purchased from Alfa Aesar. Regioregular poly(3-hexylthiophene) (P3HT) was purchased from Rieke Metals and used without purification. Indium-doped tin oxide (ITO) coated glass slides (sheet resistance = 10 Ω/□) were purchased from Nanocs (New York, NY) and cut into 1 in. by 1 in. square pieces. High purity (99.999%) metal (Au, Ag, and Cu) wires used for thermal evaporation were purchased from Alfa Aesar.

2.2. Sol−Gel Synthesis of TiO_2. TiO_2 thin films were synthesized from TBT precursor by a sol−gel method.[23] Use of TBT as a precursor helps to avoid the fast hydrolysis reaction in air that can result in poor control over the crystallite size and morphology of the TiO_2 particles.[24] First, 10 mL of TBT was dissolved in 100 mL of anhydrous ethanol. After 30 min of vigorous stirring, 10 mL of glacial acetic acid (CH_3COOH) was added to stabilize the gel, 10 mL of 2,4-pentanedione was added to promote uniform particle size distribution, and finally 10 mL of deionized water was added; the mixture was stirred at room temperature for 30 min before each reagent was added. The final sol was aged for at least a day before use.

2.3. Hybrid Solar Cell Fabrication. ITO-coated glass substrates were patterned by slow etching in a mixture of 75% deionized water, 20% HCl, and 5% HNO_3. The substrates were then rinsed with deionized water and cleaned by successive sonication in aqueous detergent, deionized water, acetone, and isopropanol. The cleaned substrates were dried in flowing nitrogen and treated with oxygen plasma for 15 min in a Harrick PDC-32G plasma cleaner. Next an electron transporting thin film of TiO_2 was deposited on the ITO substrate by spincoating the aged TiO_2 sol−gel at 3000 rpm for 20 s. After slow drying in air, the substrates were sintered in air at 450 °C for 30 min and cooled slowly to room temperature. The sintered TiO_2 films were transparent with a thickness of around 60 nm, as measured with a Dektak 3 surface profilometer and a scanning electron microscope (SEM, Hitachi S-5500).

The TiO_2-coated substrates were transferred into an argon-filled glovebox and heated at 100 °C for 15 min to remove the residual water. Unless otherwise specified, all subsequent cell fabrication steps were carried out in argon. Ten milligrams of P3HT was dissolved in 1 mL of chlorobenzene by stirring at 50 °C for 2 h and the resulting solution was filtered through a 0.20 μm pore size PTFE membrane syringe filter (Pall Life sciences). To form the hole transporting layer on TiO_2, P3HT films of 120−150 nm thickness were obtained by spincoating at a speed of 1500 rpm for 60 s. After slowly drying the films in a Petri-dish, the P3HT−TiO_2 composites were obtained by melt infiltrating P3HT into the TiO_2 layer at 185 °C in argon for 8 min. The device was completed by depositing a 2 × 3 matrix of 150 nm thick metal (Au, Ag, or Cu) electrodes at vacuum levels better than 1×10^{-7} Torr and a deposition rate of 1−2 Å/s inside a JEOL thermal evaporator. The active area of the hybrid solar cells was 3 mm × 3 mm. For cells with annealed Cu electrode, the thermally evaporated Cu film was annealed at 150 °C for 15 min in air.

2.4. Characterization Techniques. Tapping mode atomic force microscopy (AFM) imaging was carried out with a Nanoscope IIIa Dimension 3100. Scanning electron microscopy (SEM) images were

collected with a Hitachi S-5500 SEM. Glancing incidence X-ray diffraction (GIXRD) analysis was performed with a Rigaku Ultima IV diffractometer operating in parallel beam (PB) mode at 40 kV and 44 mA with CuKα radiation (λ = 1.54 Å) in the 2θ range of 20 to 80° at a step of 0.02° and a glancing angle of 0.5°. XPS studies were conducted with a Kratos analytical spectrometer using monochromatic Al Kα X-ray source. The charging effect was corrected with the binding energy of adventitious C 1s signal at 284.8 eV. A Shirley type nonlinear background was subtracted and peak deconvolution was performed using Gaussian−Lorentzian curves. Depth profiling analysis with XPS was carried out by rastering an Ar^+ ion beam on an area of 2 mm × 2 mm. The Ar^+ ion gun was operated at 4 kV and the extractor current was maintained at 75 μA during the sputtering process, resulting in an average sputtering rate of 4 Å/s during these experiments.

Solar cell current density−voltage ($J-V$) characteristics were measured under both argon atmosphere inside a MBraun glovebox (H_2O and O_2 < 0.1 ppm) and ambient conditions, with a Keithley 2400 source measurement unit. No UV blocking filter was used under both test conditions.[13] The solar cells were illuminated using an Oriel 91160 300 W solar simulator as the excitation source (100 mW/cm^2 white light illumination under AM 1.5G conditions). The solar cell test and measurement system was fully automated and photovoltaic performance parameters like open-circuit voltage (V_{oc}), short-circuit current density (J_{sc}), and fill factor (FF) that determine the overall power conversion efficiency of a solar cell were automatically computed by an in-house developed LabVIEW software. Photovoltaic parameters were measured for a series of cells and the values were found to be reproducible. The stability of these cells during continuous illumination in inert and ambient conditions was studied by tracking and recording these photovoltaic parameters every minute. Prior to these tests, the cells were stabilized by storing in argon and air respectively, for up to 2 h in the dark.

3. RESULTS AND DISCUSSION

3.1. TiO_2 Thin Film Characterization. The TiO_2 surface is an important component of this study. It was therefore necessary to obtain TiO_2 films of reproducible thickness, grain size, and morphology on all the hybrid solar cell devices tested in this study. In order to avoid charge carrier recombination, hybrid solar cell devices require TiO_2 layers of thickness on the order of 100 nm or less.[14] The sol−gel process is ideal for preparing TiO_2 films of the requisite thickness, but the fast hydrolysis reaction of common sol−gel precursors like titanium isopropoxide (TIP) can make the control of the size of TiO_2 nanoparticles rather difficult.[23,24] Accordingly, a slow hydrolyzing tetrabutyl titanate precursor was chosen instead of the commonly used TIP precursor. As the number of carbon atoms on the alkoxide group increases the hydrolysis rate slows down, offering a good control over the TiO_2 particle size.[25] The use of glacial acetic acid in the sol−gel reaction further slows down the hydrolysis process by acting as a chelating agent and changing the butoxide precursor at the molecular level. As a result, the size and morphology of the TiO_2 nanoparticles formed in the sol could be controlled.

The hybrid solar cells in this work employed a 60 nm thick TiO_2 layer obtained by sintering the spincoated TiO_2 sol−gel at 450 °C. The AFM image shown in Figure S1 in the Supporting Information suggests that the sol−gel process resulted in TiO_2 particles of ∼50 nm. The GIXRD pattern of the TiO_2 films grown on ITO substrate is shown in Figure S2 in the Supporting Information. The pattern displays a dominant peak at 25.4° corresponding to the (101) reflection of anatase TiO_2.[26] This suggests that the crystalline TiO_2 film used in our hybrid solar cells has a preferred orientation along the [101] direction. Furthermore, the absence of rutile peaks in the GIXRD pattern confirms that pure anatase TiO_2 films were obtained under these processing conditions.

3.2. Photovoltaic Performance. For this work, current density−voltage ($J-V$) curves of P3HT−TiO_2 hybrid solar cells were measured under argon (inert) and oxygen rich (ambient) conditions. Prior to these tests, the cells were stabilized by storing, respectively, in argon and air for up to 2 h in the dark. These $J-V$ curves shown in Figure 3 under dark and AM 1.5 G

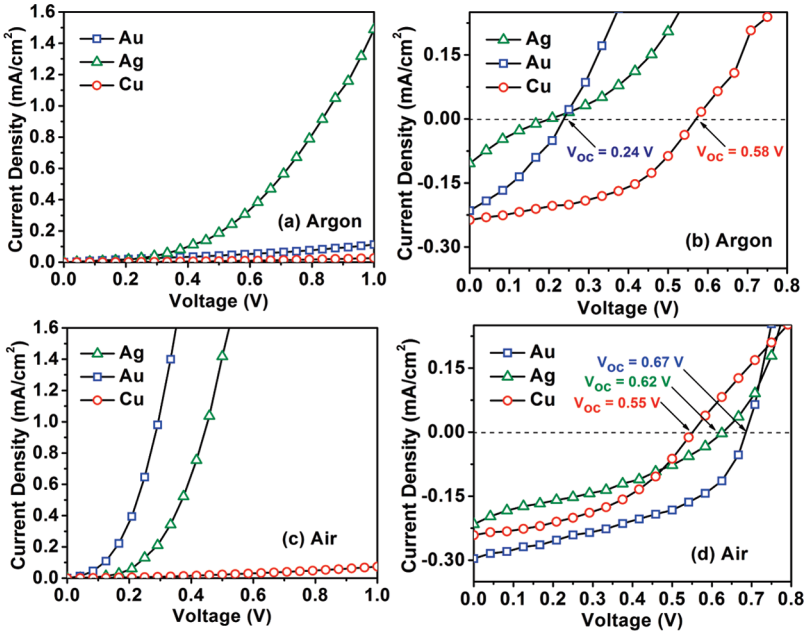

Figure 3. Dark $J-V$ characteristics of P3HT−TiO_2 hybrid solar cells in (a) argon and (c) air. Illuminated $J-V$ characteristics of P3HT−TiO_2 hybrid solar cells in (b) argon and (d) air.

Table 1. Comparison of Illuminated $J-V$ characteristics of P3HT−TiO_2 Hybrid Solar Cells in Argon and Air

electrode	V_{oc} (V)	J_{sc} (mA/cm^2)	fill factor (%)	efficiency (%)
		Argon		
Au	0.24	0.23	33	0.018
Ag	0.2	0.1	19	0.004
Cu	0.58	0.2	48	0.06
		Air		
Au	0.67	0.3	30	0.06
Ag	0.62	0.21	34	0.044
Cu	0.55	0.24	45	0.059

illumination are comparable to those obtained from similar interfacial prototype devices reported in the literature.[7,9,10] Our previous work examined the effect of various electrodes on the photovoltaic parameters of P3HT−TiO_2 hybrid solar cells and demonstrated the use of Cu as a hole-collecting electrode, in addition to the commonly used Au and Ag electrodes.[22] Accordingly, we have introduced the metal counter electrode as an experimental variable in this work.

Panels a and c in Figure 3 compare the dark $J-V$ characteristics measured under inert and ambient conditions. The Au- and Ag-based cells exhibit faster dark current onset (∼0.2 V) and an order of magnitude higher dark current values than those based on Cu. On exposing these cells to ambient atmosphere, both the Au- and Ag-based cells show an order of magnitude increase in dark current, with lower diode turn-on voltages. It must be noted that the hybrid solar cells with the Cu electrode were almost unaffected by this change in atmosphere. We subsequently compared the illuminated $J-V$ characteristics of these hybrid solar cells under inert and ambient conditions. As shown in Figure 3b, both Au- and Ag-based cells show poor open-circuit voltage (V_{oc}) values of 0.24 and 0.2 V, respectively, under inert atmosphere. When exposed to air, the V_{oc} values increased to 0.67 and 0.62 V, respectively, for the Au- and Ag-based cells (Figure 3d). This dependence of V_{oc} on oxygen has commonly been reported in the literature for hybrid solar cells based on TiO_2.[9,10] These photovoltaic parameters are summarized in Table 1.

Inside an inert atmosphere, oxygen vacancies can be created on the surface of semiconductor oxides like TiO_2. Such defects act as donors of free electrons and reduce photovoltaic parameters like V_{oc} in an environment devoid of oxygen. Furthermore, removal of oxygen from the surface of TiO_2 results in the reduction of Ti^{4+} ions to Ti^{3+} on the oxide surface.[9,10,19] A lack of oxygen can also reduce the number of free charge carriers in hole-conducting polymers like P3HT, thereby making it less p-type.[20] As seen in Figure 2, coupling these changes will result in a lowering of the contact potential at the P3HT−TiO_2 junction, thereby decreasing V_{oc} and degrading the photovoltaic properties in the absence of oxygen. On exposure to air, the Ti^{3+} species slowly oxidizes back to Ti^{4+} and the changes seen in Figure 2 are reversed. This reasoning is further corroborated by Figure 3d which indicates that V_{oc} increases on exposure to ambient atmosphere, wherein oxygen gets readsorbed onto the oxide surface and the oxygen vacancies in TiO_2 get eliminated. The free charges in P3HT are also restored on exposure to air. This reasoning is further supported by the improvement seen in the photovoltaic performance of all the cells during continuous testing under ambient conditions (see Figure S3 in the Supporting Information).

Surprisingly, Cu-based cells work consistently well both under inert and ambient conditions. As seen in panels b and d in Figure 3, Cu-based cells display comparable V_{oc} values under both these conditions. This observation seems to suggest that Cu can successfully reverse the changes occurring at the P3HT−TiO_2 interface in the absence of oxygen. To further probe this phenomenon, we recorded the variations of photovoltaic parameters (V_{oc}, J_{sc}, and FF) as a function of time for the hybrid solar cells employing Au, Ag, and Cu electrodes. These lifetime-analysis experiments were performed under continuous AM 1.5 G illumination (100 mW/cm^2) inside an argon atmosphere. As shown in Figure 4 and summarized in Table 2, photovoltaic parameters were found to degrade in the absence of oxygen. For devices employing Au and Ag electrodes, V_{oc} values decreased to almost zero (few tens of millivolts) in about 5 min, as has been reported previously in the literature.[9,10] Compared to V_{oc}, the J_{sc} and FF values for both Au- and Ag-based cells were stable throughout the test duration. This differs from some literature reports on P3HT−TiO_2 based hybrid solar cells, in which J_{sc} values quickly declined with time and reached almost zero in the absence of oxygen.[11] In our hybrid devices, we observe more stable J_{sc} values, whereas the V_{oc} values quickly decline as reported in.[9,10] The exact reason for this difference is not clear; one of the reasons could be the absence of an UV blocking filter in our experiments,[13] and it will be the subject of further study.

As efficiency is calculated based on the product of these three photovoltaic parameters, the overall hybrid solar cell efficiency can fall to zero, if any one of these parameters approaches zero. Consequently, the efficiencies of both the Au- and Ag-based cells decay to almost zero within 5 min of testing in argon atmosphere. In contrast, the Cu-based cells showed good stability during testing in the absence of oxygen. Although the photovoltaic parameters initially declined, their values quickly stabilized to a nonzero value. Furthermore, it was found that annealing the Cu layer in air at 150 °C for 15 min result in remarkable stability during continuous testing in argon atmosphere. As seen in Figure 4, the V_{oc} values stabilize at a high value of ∼0.6 V with hardly any decline during the testing. The J_{sc} and FF values stabilized, respectively, at 0.3 mA/cm^2 and 50%, resulting in a stable efficiency value of ∼0.1% during 1 h of continuous testing in argon. $J-V$ curves corresponding to the photovoltaic data in Figure 4 are shown in Figure S4 in the Supporting Information.

In summary, our results suggest that the P3HT−TiO_2 hybrid solar cells employing Cu electrodes exhibit improved stability during continuous illumination in the absence of oxygen compared to the Au- and Ag-based cells. In addition, when the Cu electrode was annealed, the solar cells exhibited remarkable stability throughout the test duration. The use of Cu electrode seems to successfully counter the complex effects of changes taking place at the P3HT−TiO_2 junction in the absence of oxygen. Although we have tested our stable Cu-based hybrid solar cells for 1 h under continuous illumination in argon, it must be noted that these cells were in an inert atmosphere for a total of 3 h (including the 2 h stabilization period before testing). We are currently working on developing a temperature and humidity controlled test bed to evaluate the performance of these cells over longer durations. Our findings were further explored by employing a series of experiments and characterization techniques as outlined below.

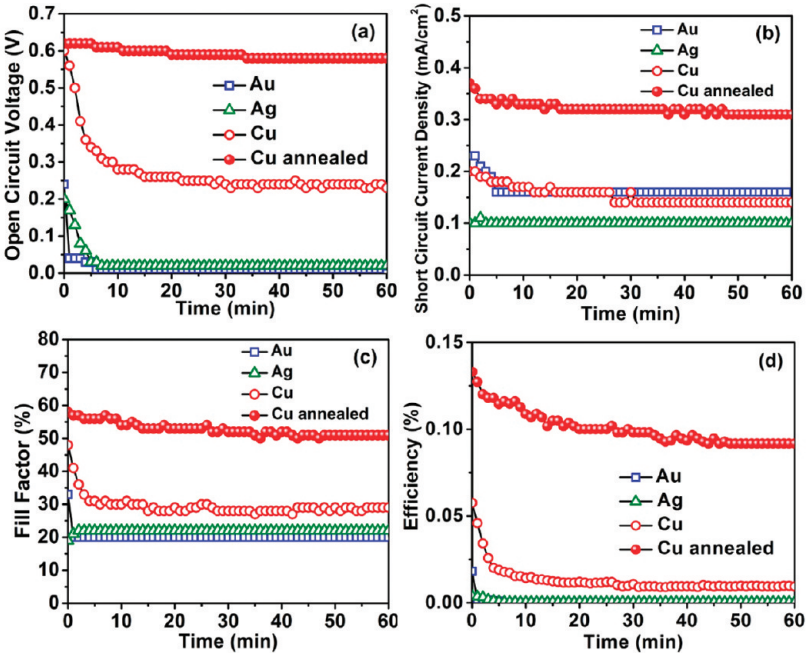

Figure 4. Variation of (a) V_{oc}, (b) J_{sc}, (c) FF, and (d) efficiency during continuous illumination in argon.

Table 2. Summary of Photovoltaic Parameters during Continuous Testing in Argon

electrode	V_{oc} (V)	J_{sc} (mA/cm^2)	fill factor (%)	efficiency (%)
		Start of Test		
Au	0.24	0.23	33	0.018
Ag	0.2	0.1	19	0.004
Cu	0.58	0.2	48	0.06
Cu annealed	0.62	0.37	58	0.133
		End of Test		
Au	0.03	0.15	20	0.001
Ag	0.03	0.08	22	0.001
Cu	0.24	0.14	30	0.01
Cu annealed	0.59	0.33	52	0.101

3.3. XPS Depth Profiling Analysis of Hybrid Solar Cell Interfaces. As evident from the stability data in Figures 4, V_{oc} appears to be the photovoltaic parameter most affected by the complex interplay between oxygen and TiO_2 surface. As V_{oc} is determined by the difference in energy between the quasi Fermi levels of P3HT and TiO_2, it is only logical to investigate if the use of a Cu counter electrode is modifying this interface.[9,10] Instead of simulating this interface by creating a separate sample, we carried out XPS depth profiling analysis on a working P3HT−TiO_2 hybrid solar cell to study in situ the P3HT and TiO_2 layers, and the interface between them. As a surface characterization tool, XPS is widely popular for studying polymer solar cells and a number of recent works have used this technique to study aspects like degradation in presence of water and oxygen.[7,27−30] XPS can provide chemical bonding information based on measured shifts in the binding energies. With a combination of depth profiling and excellent depth resolution, XPS becomes a powerful tool to elucidate the nature of different layers inside a hybrid solar cell and the interfaces between them.

We start with the analysis of the top metal surface of the hybrid solar cell and then use an Ar^+ gun to sputter through the various layers of the solar cell (see Figure S5 in the Supporting Information). Depth profiling is carried out by collecting XPS spectra from each depth level. The intensity of Au 4f, Ag 3d, Cu 2p, S 2p, and Ti 2p signals were used to monitor progress of the sputtering process. The sputtering rate depends on the material being sputtered. Hard materials like semiconductor oxides are more difficult to sputter than soft materials like polymer films. The thickness of various layers obtained using cross-sectional SEM image in Figure S5 in the Supporting Information was used to calibrate the sputtering rate of the Ar^+ gun to 2 Å/s in the metal electrode, 2−3 Å/s in the polymer, and <1 Å/s in the TiO_2 layer.

Figure S6 in the Supporting Information depicts the Au 4f, Ag 3d, and Cu 2p XPS spectra corresponding to the Au, Ag, and Cu metal electrode surfaces on the hybrid solar cells being studied. Examination of the Au and Ag spectra did not reveal changes in the shape or appearance of additional peaks compared to the pristine metals. Figure S6(c) in the Supporting Information shows that the Cu $2p_{1/2}$ peak in the Cu electrode samples occurs at a binding energy of 932.5 eV, which agrees well with the value of 932.4−932.5 eV reported in literature. However, in the case of the annealed Cu electrodes in Figure S6(c) in the Supporting Information, additional peaks appear at higher binding energies, which are close to the reported range of satellite peak positions for copper oxides (Cu_2O and CuO).[31] The annealing step also introduces morphological changes to the Cu electrode, i.e. the annealed Cu electrode has larger grain size (see Figure S7 in Supporting Information), which implies smaller grain boundary area. Oxygen can diffuse much faster through grain boundaries compared to that in the bulk. This suggests that in the cells with annealed Cu electrode, less oxygen will diffuse out of the cell because of smaller grain boundary area, thereby reducing the formation of oxygen vacancies on TiO_2 and improving the cell stability.[32,33] As mentioned earlier, inside an inert atmosphere,

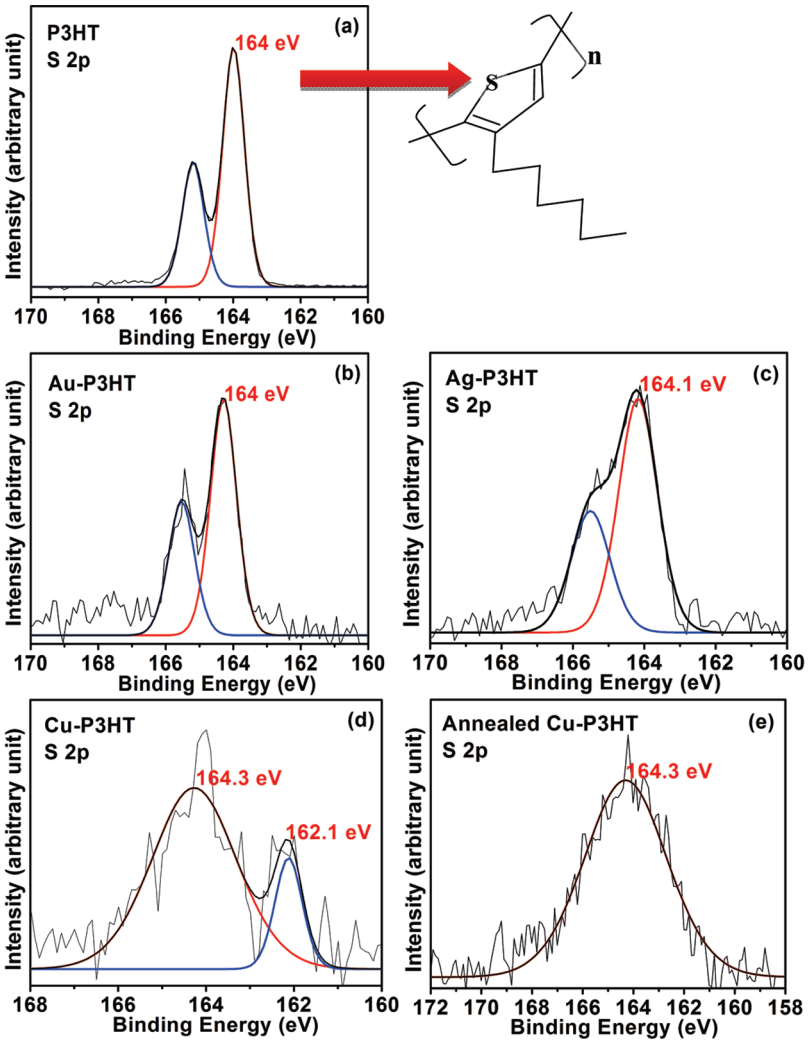

Figure 5. XPS spectra of metal-P3HT: (a) S 2p spectrum of P3HT, with the inset showing the chemical structure of P3HT, (b) S 2p spectrum of Au−P3HT interface, (c) S 2p spectrum of Ag−P3HT interface, (d) S 2p spectrum of Cu−P3HT interface, and (e) S 2p spectrum of annealed Cu−P3HT interface.

oxygen vacancies are created on the surface of semiconductor oxides like TiO_2, and such defects can act as donors of free electrons and reduce device performance.

On sputtering through the top metallic layer, the intensity of the metal signal starts to decrease and the intensity of the signal from the S 2p peak increases, suggesting the appearance of the P3HT layer, which starts at an approximate depth of 150 nm. The XPS S 2p spectrum of pristine P3HT in Figure 5a clearly indicates the presence of only one type of S, which is reflected by the S $2p_{1/2}$ and S $2p_{3/2}$ peaks, respectively, at 165.1 and 164 eV. These dual peaks with an intensity ratio of 1:2 are attributed to spin orbit coupling. As seen in Figure 5b, the deposition of Au on P3HT did not significantly alter the shape or intensity of the S 2p signal. There is no shift in the peak position, peak broadening, or appearance of new components that can suggest the presence of a region where the metal and the S atom on P3HT have reacted. Unlike Au, the deposition of Ag considerably broadens the shape of the S 2p signal from P3HT as seen in Figure 5c, suggesting a relatively weak interaction between the Ag atoms and the S atoms on P3HT.

Interestingly, the largest change in the XPS spectrum is seen in the case of Cu. The deconvoluted S 2p spectrum in Figure 5d clearly shows a new peak appearing at a lower binding energy of 162.1 eV. This new component located at −2.2 eV relative to the pristine P3HT signal suggests the formation of copper sulfides, which confirms that Cu has bonded with S, thereby donating some electron density to the thiophene ring. The unreacted S atoms on P3HT show a peak at 164.3 eV, which is shifted by +0.3 eV compared to the pristine P3HT spectrum. This increase in binding energy can be attributed to the Cu−S bonding, which results in a redistribution of electronic density and causes increased nuclear screening on the core electrons of unreacted S atoms.[34,35] These results suggest that compared to Cu, the reactivity of Ag is much weaker and Au appears chemically inert. Although the chemisorption of S containing alkanethiols onto Au surfaces is commonly used in the preparation of self-assembled monolayers (SAMs), such a bond is generally weaker than the one formed by the chemical reaction between Cu and S.[36] We believe that the improved photovoltaic stability of cells fabricated with Cu electrodes can be partly attributed to this chemical bonding between Cu and the S atoms of P3HT to give copper−sulfur complex or copper sulfide-like species. This chemical bonding drives a vertical segregation of P3HT toward the hole-collecting Cu top electrode.[22] As annealing tends to

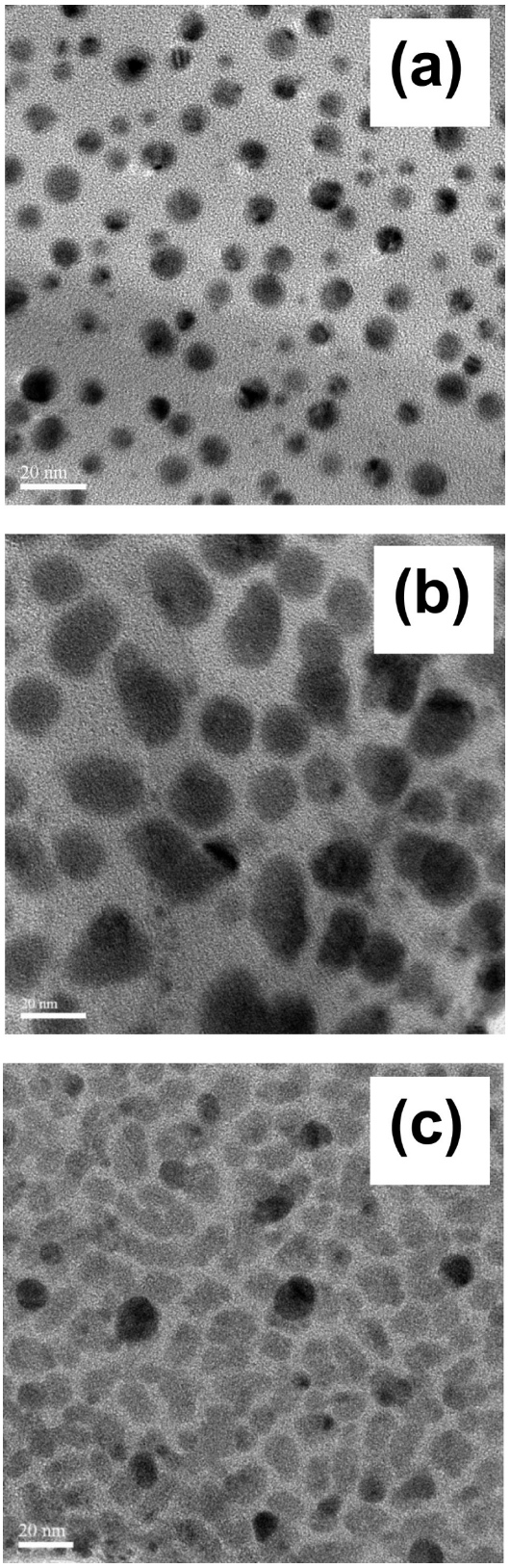

Figure 6. TEM image of (a) Au−P3HT, (b) Ag−P3HT, and (c) Cu−P3HT interface.

strengthen chemical bonds, the remarkable improvement in stability of cells made with annealed Cu electrode can be attributed to a strengthening of the Cu−S bonding. In fact, the

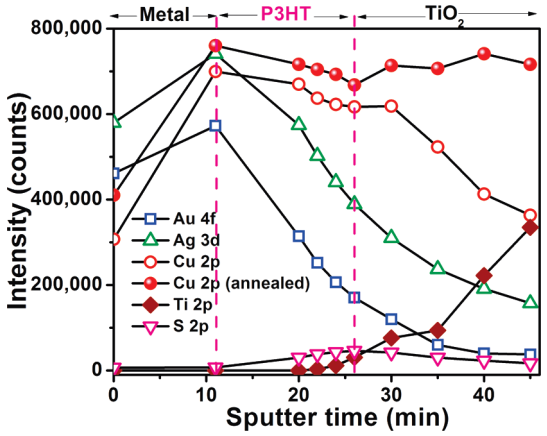

Figure 7. XPS depth profile of electrode metal inside a P3HT−TiO_2 hybrid solar cell.

XPS signal for annealed Cu shows a very broad S 2p peak which confirms this hypothesis (Figure 5e). There is additionally an electric field induced effect, because hole injection from Cu electrode has been reported to be more efficient than that from Au in Organic Field Effect Transistors (OFETS).[37]

TEM imaging was conducted to further examine this P3HT−metal interface. A very dilute (10 μg/mL) P3HT solution was spincast at speeds >5000 rpm onto a glass slide with a carbon TEM grid stuck on it. A very thin (2 −5 nm) metal (Au, Ag, and Cu) layer was deposited onto the polymer coated grid to create regions on the TEM grid where it is possible to observe the polymer−metal interface. TEM images in Figure 6 indicate that although Au and Ag atoms form clusters, the Cu atoms uniformly wet the P3HT surface. This can also be attributed to the greater tendency for Cu to react with S atoms on P3HT as explained above. Wettability of Ag films seems to fall between that of Au and Cu films, agreeing with the knowledge that chemical reactivity of these metals vary as Cu > Ag > Au. The formation of such copper−sulfur complexes could also facilitate the migration of these Cu atoms deeper into the various layers of solar cell.[7,38] The initial ohmic behavior observed in the dark $J-V$ characteristics of Cu-based cells in panels a and c in Figure 3 can be explained by the presence of such a copper−sulfur complex.[39] Heating caused by illumination may break the copper sulfide like species, thereby eliminating device shunting as indicated in Figure S8 in the Supporting Information

As the Ar^+ beam continues to sputter through the hybrid solar cell, there is an increase in the signal from Ti 2p and a decrease in the signal from S 2p, suggesting the appearance of the P3HT−TiO_2 interface. Interestingly, signal strength from Au 4f, Ag 3d, and Cu 2p does not fall to zero at this depth. This suggests that the atoms from these top metal electrodes tend to migrate deep into the hybrid solar cell and can even diffuse all the way up to the TiO_2 surface. It is evident from Figure 7 that although Au and Ag atoms also diffuse up to the TiO_2 layer, their XPS signal intensity at this depth is less than half of the signal intensity of Cu atoms. Referring back to the TEM images in Figure 6, the inability of Cu atoms to form clusters on P3HT seems to enable them to diffuse into the polymer. Once clusters form, additional atoms tend to add to these clusters rather than diffuse into or react with P3HT. This could explain why the XPS signal intensity from Au and Ag atoms is lower than that of Cu deeper inside the solar cell. As the chlorobenzene solvent used to

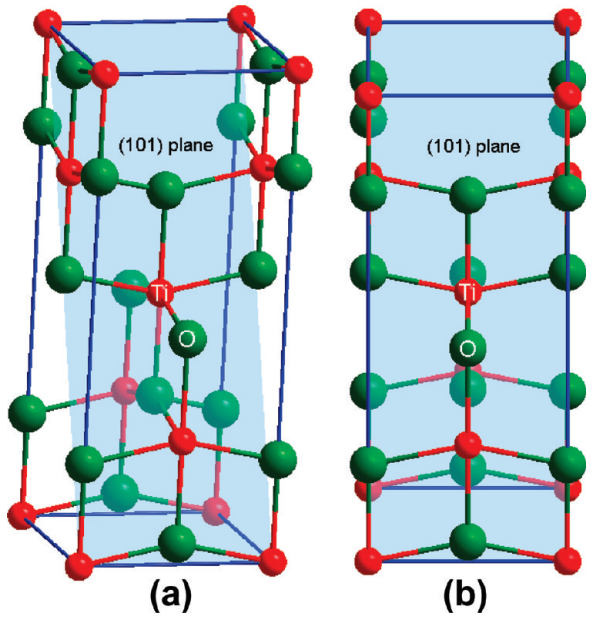

Figure 8. (a) Structure of anatase TiO_2 and (b) a view along [101].

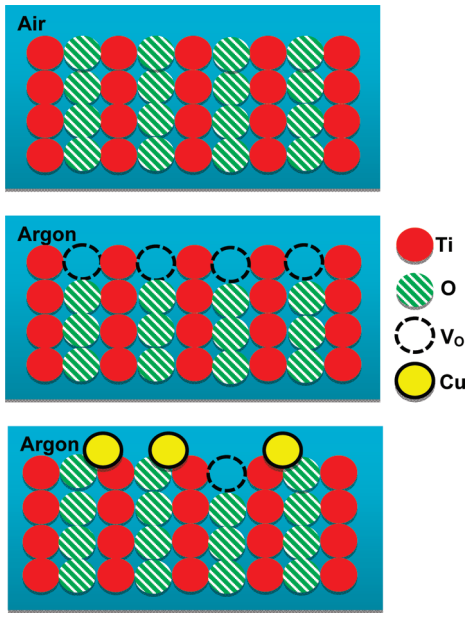

Figure 9. Depiction of the reaction of Cu with TiO_2 surface species. V_O denotes oxygen vacancies.

prepare the P3HT films does not dissolve Cu, it is highly probable that the transport of Cu deep inside the solar cell is aided by its ability to chemically bond with the S atoms on P3HT.[38]

Knowing that Cu is a reactive metal, the question now arises whether Cu would react with TiO_2. In fact, according to the Joint Committee on Powder Diffraction Standards (JCPDS) database, while there are only two Ag−TiO_2 compounds, more than seven Cu−TiO_2 compounds have been reported. There are, however, no Au−TiO_2 compounds known. This further suggests a stronger chemical interaction of Cu with TiO_2, when compared to Au and Ag. To understand further, we examined the XPS Ti 2p binding energy at the P3HT−TiO_2 interface for the case of each of these three electrode metals. The XPS spectra (see Figure S9 in the Supporting Information) indicate +0.51 eV and +0.66 eV shift in the Ti 2p binding energy levels in the case of the Cu and annealed Cu cells, respectively, compared to that found with the Au and Ag electrodes. These positive shifts in the binding energy values suggest a less reduced Ti, which in turn may imply that there are less vacancies on the TiO_2 surface in the hybrid solar cells made with Cu and annealed Cu electrodes.[24,26] Such a strong interaction between TiO_2 and Cu atoms can explain the improved stability exhibited by these cells in the absence of oxygen.

These results opens up the possibility that Cu atoms from the top metal electrode can diffuse up to the TiO_2 layer and subsequently fill up the vacancies on the surface of TiO_2 as in eq 1

$$TiO_{2-\delta} \xrightarrow{x\mathrm{Cu} + \delta O_2} \mathrm{Cu}_x TiO_2 \qquad (1)$$

Figure 8 illustrates the structure of anatase TiO_2, highlighting the dominant (101) plane where oxygen vacancies can occur. However, as indicated in Figure 9, this reaction is a surface phenomenon and does not change the bulk properties of TiO_2 such as the band gap.[26,40] This reasoning is further confirmed as we do not see any decrease in V_{oc} during continuous testing of the annealed Cu-based cells (Figure 4a). The resulting Cu_xTiO_2 surface without oxygen defects appears to be more stable than TiO_2 with oxygen vacancies. This can also explain why TiO_2 based hybrid solar cells with Cu electrode are remarkably stable even in the absence of oxygen. Annealing can further increase the driving force for this surface reaction between Cu and TiO_2, thereby explaining the remarkable improvement in stability observed on annealing the Cu electrode. The strong XPS signal intensity suggests that there are a considerable number of Cu atoms at the surface of TiO_2. Not only is the signal from Ag atoms weak, being a less reactive metal than Cu, it is likely that Ag will not fill up the vacancies on TiO_2 surface like Cu does. The findings discussed here suggest that the interaction of Cu with P3HT and TiO_2 at the metal−polymer and polymer−TiO_2 interfaces make a synergistic contribution toward improving the stability of the hybrid solar cells. Figure S10 in the Supporting Information further suggests that in addition to the stability improvement of the P3HT−TiO_2 hybrid solar cells, Cu can also be pursued as a low-cost alternative to the noble metal electrodes used in other types of polymer solar cells.[41,42]

3.4. Role of Polymer on Stability. It is widely reported that annealing improves the crystallinity of P3HT.[43,44] This raises the question of whether the improvement in stability seen on annealing Cu can be attributed to this effect. However, it is interesting that the use of Cu as electrode improves the stability even in unannealed cells (Figure 4). In fact, as shown in Figure S4 in the Supporting Information, the Au- and Ag-based cells also exhibit improvement in stability on annealing the respective metal layers, as previously reported in the literature.[14] However, this stability improvement is small compared to the improvement seen when using annealed Cu electrodes (Figure 4). Furthermore, ohmic behavior is seen in these cells after continuous testing in argon. Being the more reactive metal, the interaction of Cu with P3HT and TiO_2 at the metal−polymer and polymer−TiO_2 interfaces is stronger compared to that with Au and Ag. Annealing the Cu electrode can further strengthen these interfacial interactions. We, therefore, conclude that the improvement in stability reported here can be attributed to a

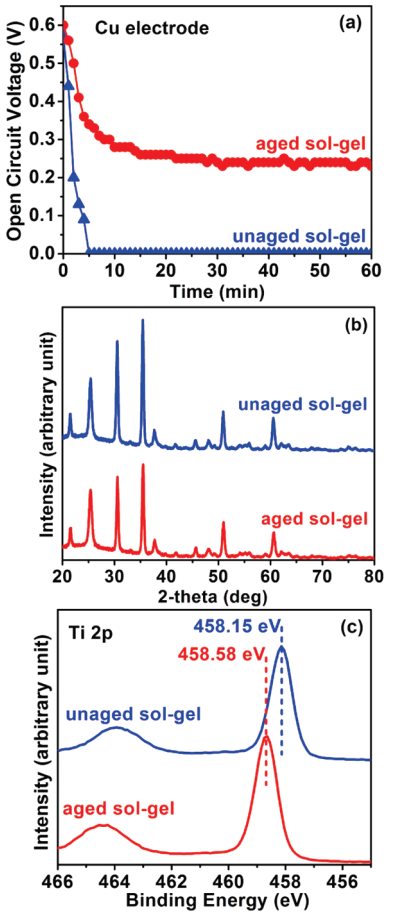

Figure 10. Effect of TiO_2 sol−gel aging on stability: (a) variation of V_{oc} in argon, (b) GIXRD plots, and (c) XPS Ti 2p spectra.

combination of P3HT crystallization and the effect of Cu. Our future work will study the effect of Cu in cells incorporating more stable polymers like −COOH-functionalized polythiophenes[13] to gain further understanding on this issue.

3.5. Role of TiO_2 Surface on Stability. It was recently reported that the application of TiO_2 in its rutile phase enhanced long-term stability of hybrid solar cells.[11] In this regard, XPS evidence about the interaction between Cu and the TiO_2 led us to examine the surface of the TiO_2 in greater detail. The objective was to determine whether the stability exhibited by Cu electrode would vary depending on the aging conditions of the TiO_2 sol−gel. The aging process involves storing the freshly prepared sol−gel in the dark under ambient conditions for 2−3 weeks. As seen in Figure 10a, V_{oc} of the hybrid solar cells fabricated with unaged TiO_2 declined within 5 min of testing in the absence of oxygen. Comparison of the GIXRD patterns in Figure 10b shows no difference between these two types of TiO_2, signifying that a surface phenomenon is responsible for the observed change in stability. Characterization techniques like XRD cannot pick up such surface phenomena, which further confirms the choice of XPS as the characterization tool for this study. XPS Ti 2p signals from both aged and unaged TiO_2 are shown in Figure 10c. The Ti 2p levels of unaged TiO_2 is shifted by −0.43 eV compared to the aged TiO_2. This shifted value is closer to the binding energy of Ti^{3+} than Ti^{4+}, suggesting that the Ti is more reduced. In other words, there are more vacancies on the TiO_2 surface in this case. Such defects can then act as donors of free electrons and cause the quick decline in V_{oc} seen in Figure 10a. From a practical standpoint, this finding demonstrates that the aging process contributes to determine the surface characteristics of TiO_2, which in turn determines the hybrid solar cell properties. The stable Cu-based cells in Figure 4 used a TiO_2 sol−gel that was aged for at least a day.

4. CONCLUSIONS

In summary, we have shown that the use of Cu as the top hole-collecting electrode can improve the stability and performance of P3HT−TiO_2-based hybrid solar cells in the absence of oxygen. Data from photovoltaic device performance tests and XPS analysis attribute this improvement to the tendency of Cu to form strong sulfide-like complexes with the S atoms on P3HT, thereby inducing a chemically driven vertical segregation of P3HT toward the hole-collecting metal electrode. Additionally, XPS depth profiling analysis shows that Cu atoms can diffuse up to the TiO_2 layer and fill up oxygen vacancies on the TiO_2 surface, thus eliminating defects that can act as donors of free electrons and degrade photovoltaic performance in an inert atmosphere. These findings suggest that the interaction of Cu with P3HT and TiO_2 at the metal−polymer and polymer−TiO_2 interfaces make a synergistic contribution toward improving the stability of the hybrid solar cells. The stability of these hybrid devices further depends on a complex array of parameters that are heavily influenced by the cell fabrication steps, synthesis, morphology, phase and chemistry of TiO_2, and annealing conditions of P3HT. Nevertheless, this study represents a preliminary work on the effect of Cu on the stability of P3HT−TiO_2-based hybrid solar cells in an inert atmosphere. Future work in our laboratory will apply the insights gained from this study to fabricate optimized devices that exhibit higher efficiencies.

■ ASSOCIATED CONTENT

Supporting Information. AFM image and GIXRD pattern of TiO_2 film, photovoltaic stability data in air, $J-V$ curves of photovoltaic stability tests in argon, cross-sectional SEM image of hybrid solar cell, SEM image of electrode, XPS spectra of metal and Ti 2p, advantages of Cu electrode, and photovoltaic data summary tables. This material is available free of charge via the Internet at http://pubs.acs.org/.

■ AUTHOR INFORMATION

Corresponding Author

*Phone: 512-471-1791. Fax: 512-471-7681. E-mail: rmanth@mail.utexas.edu.

■ ACKNOWLEDGMENT

This work was supported by the Welch Foundation grant F-1254. The authors also thank the National Science Foundation (Grant 0821312 and 0618242) for funding the Hitachi S-5500 Scanning Electron Microscope and Kratos Axis Ultra XPS used in this work.The authors thank Danielle Applestone and Thomas Cochell for their assistance with the XPS analysis.

■ REFERENCES

(1) Helgesen, M.; Sondergaard, R.; Krebs, F. C. *J. Mater. Chem.* **2010**, *20*, 36–60.

(2) Krebs, F. C.; Norrman, K. *ACS Appl. Mater. Interfaces* **2010**, *2*, 877–887.
(3) Chen, Li-Min; Zheng, X.; Hong, Z.; Yang, Y. *J. Mater. Chem.* **2010**, *20*, 2575–2598.
(4) Peet, J.; Heeger, A. J.; Bazan, G. *Acc. Chem. Res.* **2009**, *42*, 1700–1708.
(5) Ameri, T.; Dennler, G.; Lungenschmied, C.; Brabec, C. J. *Energy EnViron. Sci.* **2009**, *2*, 347–363.
(6) (a) Krebs, F. C.; Gevorgyan, S. A.; Alstrup, J. *J. Mater. Chem.* **2009**, *19*, 5442–5451. (b) Krebs, F. C.; Jørgensen, M.; Norrman, K.; Hagemann, O.; Alstrup, J.; Nielsen, T. D.; Fyenbo, J.; Larsen, K.; Kristensen, J. *Sol. Energy Mater. Sol. Cells* **2009**, *93*, 422–441. (c) Krebs, F. C. *Sol. Energy Mater. Sol. Cells* **2009**, *93*, 465–475.
(7) Jørgensen, M.; Norrman, K.; Krebs, F. C. *Sol. Energy Mater. Sol. Cells* **2008**, *92*, 686–714.
(8) Takayuki Kuwabara, T.; Iwata, C.; Yamaguchi, T.; Takahashi, K. *ACS Appl. Mater. Interfaces* **2010**, *2*, 2254–2260.
(9) Al-Dmour, H.; Taylor, D. M. *Appl. Phys. Lett.* **2009**, *94*, 223309.
(10) Watanabe, A.; Kasuya, A. *Thin Solid Films* **2005**, *483*, 358–366.
(11) Lira-Cantu, M.; Chafiq, A.; Faissat, J.; Gonzalez-Valls, I.; Yu, Y. *Sol. Energy Mater. Sol. Cells* **2011**, *95*, 1362−1374.
(12) (a) Lira-Cantu, M.; Krebs, F. C. *Sol. Energy Mater. Sol. Cells* **2006**, *90*, 2076–2086. (b) Lira-Cantu, M.; Norrman, K.; Andreasen, J. W.; Casan-Pastor, N.; Krebs, F. C. *J. Electrochem. Soc.* **2007**, *154*, B508–B513.
(13) Krebs, F. C. *Sol. Energy Mater. Sol. Cells* **2008**, *92*, 715–726.
(14) (a) Coakley, K. M.; McGehee, M. D. *Appl. Phys. Lett.* **2003**, *83*, 3380–3382. (b) Coakley, K. M.; McGehee, M. D. *Chem. Mater.* **2004**, *16*, 4533–4542. (c) Greene, L. E.; Law, M.; Yuhas, B. D.; Yang, P. *J. Phys. Chem. C* **2007**, *111*, 18451–18456.
(15) Chang, J. A.; Rhee, J. H.; Im, S. H.; Lee, Y. H.; Kim, H.-J.; Seok, S. I.; Nazeeruddin, Md. K.; Gratzel, M. *Nano Lett.* **2010**, *10*, 2609–2612.
(16) Ishwara, T.; Bradley, D. D. C.; Nelson, J.; Ravirajan, P.; Vanseveren, I.; Cleij, T.; Vanderzande, D.; Lutsen, L.; Tierney, S.; Heeney, M.; McCulloch, I. *Appl. Phys. Lett.* **2008**, *92*, 053308.
(17) Antoniadou, M.; Stathatos, E.; Boukos, N.; Stefopoulos, A.; Kallitsis, J.; Krebs, F. C. *Nanotechnology* **2009**, *20*, 495201–495210.
(18) Lin, Y. Y.; Chu, T. H.; Li, S. S.; Chuang, C. H.; Chang, C. H.; Su, W. F.; Chang, C. P.; Chu, M. W.; Chen, C. W. *J. Am. Chem. Soc.* **2009**, *131*, 3644–3649.
(19) (a) Di Valentin, C.; Pacchioni, G.; Selloni, A. *J. Phys. Chem. C* **2009**, *113*, 20543–20552. (b) Morgan, B. J.; Watson, G. W. *Phys. Rev. B* **2009**, *80*, 233102. (c) Papageorgiou, A. C.; Beglitis, N. S.; Pang, C. L.; Teobaldi, G.; Cabailh, G.; Chen, Q.; Fisher, A. J.; Hofer, W. A.; Thornton, G. *Proc. Natl. Acad. Sci. U.S.A.* **2010**, *107*, 2391–2396. (d) Bonapasta, A. A.; Filippone, F.; Mattioli, G.; Alippi, P. *Catal. Today* **2009**, *144*, 177–182.
(20) Taylor, D. M.; Gomes, H. L.; Underhill, A. E.; Edge, S.; Clemenson, P. I. *J. Phys. D* **1991**, *24*, 2032–2038.
(21) Abdou, M. S. A.; Orfino, F. P.; Son, Y.; Holdcroft, S. *J. Am. Chem. Soc.* **1997**, *119*, 4518–4524.
(22) Reeja-Jayan, B.; Manthiram, A. *Sol. Energy Mater. Sol. Cells* **2010**, *94*, 907–914.
(23) Xue, H.; Kong, X.; Liu, Z.; Liu, C.; Zhou, J.; Chena, W.; Ruan, S.; Xu, Q. *Appl. Phys. Lett.* **2007**, *90*, 201118.
(24) Wua, J. C. S.; Yeh, Chih-Yang *J. Mater. Res.* **2001**, *16*, 615–620.
(25) Dunuwila, D. D.; Gagliardi, C. D.; Berglund, K. A. *Chem. Mater.* **1994**, *6*, 1556–1562.
(26) Diebold, U. *Surf. Sci. Rep.* **2003**, *48*, 53–229.
(27) Norrman, K.; Madsen, M. V.; Gevorgyan, S. A.; Krebs, F. C. *J. Am. Chem. Soc.* **2010**, *132*, 16883–16892.
(28) Norrman, K.; Alstrup, J.; Krebs, F. C. *Surf. Interface Anal.* **2006**, *38*, 1302–1310.
(29) Bebensee, F.; Schmid, M.; Steinruck, H.-P.; Campbell, C. T.; Gottfried, J. M. *J. Am. Chem. Soc.* **2010**, *132*, 12163–12165.
(30) Norrman, K.; Gevorgyan, S. A.; Krebs, F. C. *ACS Appl. Mater. Interfaces* **2009**, *1*, 102–112.
(31) (a) Armelao, L.; Barreca, D.; Bertapelle, M.; Bottaro, G.; Sada, C.; Tondello, E. *Thin Solid Films* **2003**, *442*, 48–52. (b) Yoon, K. H.; Choi, W. J.; Kang, D. H. *Thin Solid Films* **2000**, *372*, 250–256.
(32) (a) Norrman, K.; Krebs, F. C. *Sol. Energy Mater. Sol. Cells* **2006**, *90*, 213–227. (b) Norrman, K.; Larsen, N. B.; Krebs, F. C. *Sol. Energy Mater. Sol. Cells* **2006**, *90*, 2793–2814. (c) Gevorgyan, S. A.; Jørgensen, M.; Krebs, F. C. *Sol. Energy Mater. Sol. Cells* **2008**, *92*, 736–745.
(33) (a) Seemann, A.; Egelhaaf, H.-J.; Brabec, C. J.; Hauch, J. A. *Org. Electron.* **2009**, *10*, 1424–1428. (b) Hauch, J. A.; Schilinsky, P.; Choulis, S. A.; Rajoelson, S.; Brabec, C. J. *Appl. Phys. Lett.* **2008**, *93*, 103306.
(34) Lachkar, A.; Selmani, A.; Sacher, E.; Leclerc, M.; Mokhliss, R. *Synth. Met.* **1994**, *66*, 209–215.
(35) (a) Vesely, C. J.; Langer, D. W. *Phys. Rev. B* **1971**, *4*, 451–462. (b) Kundu, M.; Hasegawa, T.; Terabe, K.; Yamamoto, K.; Aono, M. *Sci. Technol. Adv. Mater.* **2008**, *9*, 035011.
(36) Ning, Y.; Xie, H.; Xing, H.; Deng, W.; Yang, D. *Surf. Interface Anal.* **1996**, *24*, 667–670.
(37) Di, Chong-an; Yu, G.; Liu, Y.; Guo, Y.; Wang, Y.; Wu, W.; Zhu, D. *Adv. Mater.* **2008**, *20*, 1286–1290.
(38) (a) Godbey, D. J.; Buckley, L. J.; Purdy, A. P.; Snow, A. W. *Thin Solid Films* **1997**, *308*, 470–474. (b) Miki, N.; Tanaka, K.; Takahara, A.; Kajiyama, T. *J. Vac. Sci. Technol., B* **2000**, *18*, 313–316.
(39) Amith, A. *J. Appl. Phys.* **1979**, *50*, 1160–1162.
(40) Schaub, R.; Wahlstrom, E.; Rønnau, A.; Lægsgaard, E.; Stensgaard, I.; Besenbacher, F. *Science* **2003**, *299*, 377–379.
(41) (a) Woo, K.; Bae, C.; Jeong, Y.; Kim, D.; Moon, J. *J. Mater. Chem.* **2010**, *20*, 3877–3882. (b) Jeong, S.; Woo, K.; Kim, D.; Lim, S.; Kim, J.; Shin, H.; Xia, Y.; Moon, J. *Adv. Funct. Mater.* **2008**, *18*, 679–686. (c) Park, B.; Kim, D.; Jeong, S.; Moon, J. *Thin Solid Films* **2007**, *515*, 7706–7711.
(42) (a) Kim, C. S.; Lee, S. S.; Gomez, E. D.; Kim, J. B.; Loo, Y.-L. *Appl. Phys. Lett.* **2009**, *94*, 113302. (b) Kim, J. B.; Kim, C. S.; Kim, Y. S.; Yueh-Lin *Appl. Phys. Lett.* **2009**, *95*, 183301.
(43) Olson, D. C.; Shaheen, S. E.; Collins, R. T.; Ginley, D. S. *J. Phys. Chem. C* **2007**, *111*, 16670–16678.
(44) Ma, W. L.; Yang, C. Y.; Gong, X.; Lee, K.; Heeger, A. J. *Adv. Funct. Mater.* **2005**, *15*, 1617–1622.